

Installation and commissioning of the Deeply
Virtual Compton Scattering experiment at the
Jefferson Lab

Matthieu Beaumel

October 29, 2004

Abstract

“Physics is like sex: sure, it may give some practical results, but that’s not
why we do it.”
- Richard P. Feynmann

Acknowledgments

Firstly, I would like to thank Michel Garçon from the CEA Saclay to have given me the opportunity to come at the Jefferson Lab to work on the DVCS experiment.

François-Xavier, Malek and Jean-Marc have managed to cope with my unbearable working hours during three months. I'd like to thank them here.

The DVCS Team has always been helpful and caring. I would like to thank Eric Voutier, Catherine Ferdi and especially Pierre Bertin who also made me discover the secret places and lost beaches surrounding Newport News.

The experiment wouldn't have been the same without the hard work of the students working on it. I'd like to thank Carlos Muñoz Camacho and Alexandre Camsonne for all the help they gave me, but also for introducing me to the life of young foreigners lost in the United States. If working with them was very pleasant, discovering american lifestyle in their company was even more addicting.

And last but not least, I would particularly like to thank Franck Sabatié for all what he taught me, for his constant kindness and above all, for showing me there was definitely *life in physics*.

Contents

1	The Deeply Virtual Compton Scattering experiment	1
1.1	Goal of the experiment	1
1.2	Context of the experiment	2
1.2.1	An international cooperation at the Jefferson Laboratory	2
1.2.2	The CEBAF accelerator	2
1.3	Theory of the experiment	4
1.4	Experimental apparatus	6
1.4.1	General setup	6
1.4.2	Cryogenic target	7
1.4.3	Hall A high resolution spectrometer	7
1.4.4	Calorimeter	9
1.4.5	Proton array	13
1.4.6	Tagger	14
2	Several aspects of my work on DVCS	15
2.1	Timeline	15
2.2	Calorimeter calibration	15
2.2.1	The need for a calibration	15
2.2.2	Cross-calibration using cosmic rays	16
2.2.3	Cross-calibration using LEDs	20
2.3	Data acquisition	24
2.3.1	Challenges of data acquisition	24
2.3.2	Data acquisition electronics	25
2.3.3	Triggering procedure	28
	Conclusion	31
A	ROOT framework	33
B	Examples of ROOT offline analysis macros	35
B.1	Calibration with cosmics	35
B.2	LED shape analysis	35
B.3	Example of a VxWorks program	35
B.4	Miscellaneous pictures	35

List of Figures

1.1	Top-down view of the CEBAF.	2
1.2	Side view of the Hall A.	3
1.3	Handbag diagram of the DVCS process.	4
1.4	DVCS and BH processes are both characterized by $ep \rightarrow e'\gamma p'$	5
1.5	DVCS and BH processes interfere like in holography.	5
1.6	General setup of the DVCS experiment.	6
1.7	DVCS detector in the testing room.	6
1.8	Scattering chamber in the storage building.	7
1.9	High Resolution Spectrometers in Hall A.	8
1.10	DVCS kinematics: leptonic (green) and hadronic (yellow) planes.	8
1.11	Structure of a generic calorimeter.	9
1.12	Several blocks within the Moliere radius are hit.	10
1.13	DVCS Calorimeter in the testing room: front and back view.	11
1.14	Shower resulting from a photon hit.	12
1.15	Čerenkov shockwave.	12
1.16	Proton array schematics (left) and actual view (right).	13
1.17	Scattering chamber and beamline (in purple) position relatively to the calorimeter (green) and proton array (red and blue).	13
1.18	Tagger in position over the proton array.	14
2.1	Event produced by a cosmic in the calorimeter, viewed from the back. The numbers represent the values of the energies that were deposited in each block.	17
2.2	Stopping power of muons in copper. Cosmics in lead glass present the same profile, with a flat zone around the minimum ionization energy.	17
2.3	Event produced by a cosmic passing through the calorimeter vertically. The goal of cross-calibration is to have all the energy values in the column equalized.	18
2.4	Histogram of the means of the integrated charges on each block for cosmic calibration and fitted gaussian ($\sigma/\mu = 2.7\%$).	18
2.5	Schematics of the XY table.	20
2.6	LEDs device on the XY table.	20
2.7	3D maps of the block #131 produced by the fine-block scanning (top-down view).	21
2.8	3D maps of the block #131 produced by the fine-block scanning (isometric view).	22
2.9	Gain variation over 18 days of the different calorimeter blocks. 4 blocks are above 15%, and one above 30%.	23

2.10	Gain variation over 18 days of block #39.	23
2.11	Hall B DAQ system. Removing a single cable is likely to cause the failure of the whole system.	24
2.12	Typical pulse from a photomultiplier recorded by the ARS. . . .	25
2.13	Example of a pile-up event that the ARS is able to resolve. . . .	26
2.14	DVCS VME crates for DAQ in the testing room.	27
2.15	Side view of a VME ARS board. There are 4 ARS units with 4 channels each, giving a total of 16 channels per board.	27
2.16	DAQ setup for cosmics.	28
2.17	Schematics of the DVCS trigger.	29

Chapter 1

The Deeply Virtual Compton Scattering experiment

1.1 Goal of the experiment

Although the nucleon (proton or neutron) has been subject to intense studies since the 60s, both experimentally with scattering experiments and theoretically using QCD, we still know very little about the details of its inner structure. So far, two observables have helped us in getting a better understanding of the nucleon: the *form factors* and the *parton distributions*.

Form factors have been interpreted as the Fourier transform of the charge and magnetization distribution inside the nucleon, and parton distributions as the probability that a parton (quark or gluon) carries a particular fraction of the nucleon momentum. In essence, these two observables give us complementary but uncorrelated information: form factors tell us about the spatial location of the partons, and parton distributions about their momentum distribution.

Recently, a new theoretical framework called *Generalized Parton Distributions* (GPDs) unifying these two observables has been developed. GPDs not only contain the form factor and parton distributions information, but also correlates the momentum distribution and position of the parton. The simplest exclusive process allowing the measurement of the GPDs is the *Deeply Virtual Compton Scattering* (DVCS), where a virtual photon is scattered off a nucleon and emits a real photon in the final state. More information about the theory of DVCS can be found in section 1.3.

The “E00-110” experiment on which I had the chance to work is the first one dedicated to the investigation of GPDs using the DVCS process.

1.2 Context of the experiment

1.2.1 An international cooperation at the Jefferson Laboratory

“E00-110: DVCS at 5.75 GeV” is officially running along with its sister experiment “E03-106: DVCS on the neutron” from September 14 to November 24 in the Hall A of the Thomas Jefferson National Accelerator Facility in Newport News (Virginia). At heart, the Jefferson Lab is dedicated to hadronic physics, even if it has broadened its range of studies nowadays and is actively researching in the field of applied physics. One of the most striking aspects of the JLab consists in the fact that it is primarily an user facility for scientists worldwide. As such, it welcomes a vast international community of researchers and students. Three different experiments can be run at once in the three experimental halls linked to the accelerator facility, designated as Hall A, B and C. Each hall has its own staff and experimental schedule.

The DVCS team I joined was a close cooperation of many different institutes, with most notable contributions to the project coming from CEA Saclay (DAPNIA/SPhN), LPC Clermont Ferrand (CNRS/IN2P3), LPSC Grenoble (CNRS/IN2P3), Old Dominion University, Rutgers University and Jefferson Lab itself.

1.2.2 The CEBAF accelerator

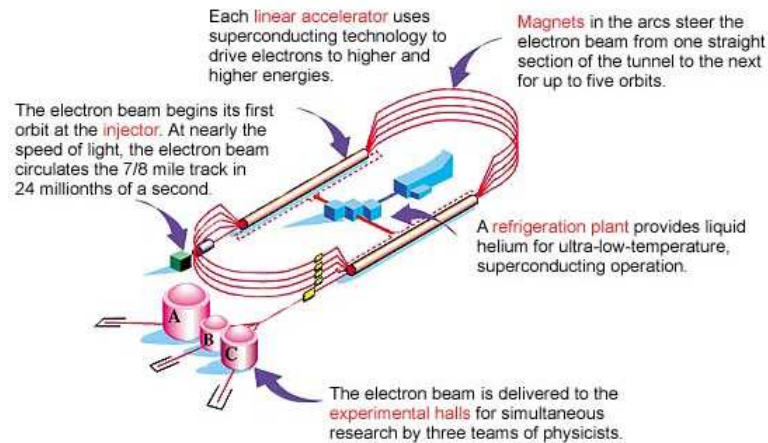


Figure 1.1: Top-down view of the CEBAF.

The racetrack-shaped accelerator is called CEBAF¹ because of its ability to deliver a continuous electron beam to the three different endstations. The CEBAF is considered as an **accelerator of a medium power**, being able to accelerate the beam up to 5.8 GeV with a maximum current of $200\mu A$. It is divided into three parts: the injector, the north and south linear accelerators and the two magnets that steer the beam.

¹Continuous Electron Beam Accelerator Facility.

The injector accelerates each electron beam pulse up to 45 MeV at a frequency of 1497 MHz. Right after their production, the pulses go through a chopping aperture which is composed of three slits of different size, one for each of the experimental halls endstations. The width of the slits determine the beam currents that are delivered to each hall.

The beam is then injected into the north linear accelerator, which accelerates the electrons by placing negatives charges behind them and positives charges in front of them. For this operation, 160 super-conducting cavities made of niobium are used. These cavities are grouped 8 by 8 into cryomodules which are cooled down by helium at 2 K provided by the Central Helium Liquefier (CHL). The total energy of acceleration given by the north linear accelerator is 400 MeV.

At the end of the north linear accelerator, the beam is bent into a semi-circle in the west magnetic recirculation arcs and enters the south linear accelerator, which gives it an additional energy of 400 MeV. At this point, the beam can either be delivered to the endstations or go in the east reticulation arcs for another run around the accelerator. Up to five revolutions in the accelerator can be made by the beam depending of the energy requests of the different halls, each turn providing an additional 800 MeV of energy. While all the beams of a different energy are traveling in the same beamline in the north and south linear accelerators, they require different bending fields in the reticulation arcs. Therefore, at the end of each linear accelerator the beams are sorted by momentum and each one goes into a different arc before being recombined again.

As seen in figure 1.2, the experimental halls by themselves are large domes of different sizes, Hall A being the largest with a diameter of 53 meters. Each one is equipped with detectors of various characteristics, giving them different experimental focuses. Hall A specializes in high resolution experiments at high luminosity thanks to its large magnetic spectrometers which will be described in section 1.4.3, Hall B is equipped with a large acceptance spectrometer with an acceptance of nearly 4π called CLAS² and runs experiments at a limited luminosity, while Hall C falls somewhere in between, having detectors with a lower momentum resolution than the ones that can be found in Hall A but covering a larger solid angle.

²CEBAF Large Acceptance Spectrometer.

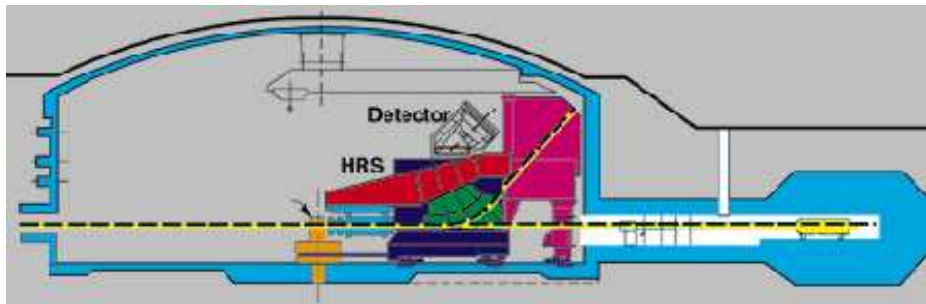


Figure 1.2: Side view of the Hall A.

1.3 Theory of the experiment

The DVCS process on the neutron can be described by two steps: the absorption of a *virtual* photon (the exchange particle of the electromagnetic interaction) by the nucleon and the immediate re-emission of a high-energy *real* photon.


$$\gamma^* p \rightarrow \gamma p' \quad (1.1)$$

γ^* being a virtual photon, and γ a real photon.

Experimentally, we can produce the DVCS process by scattering an electron on a proton, as they will exchange a virtual photon during their interaction. The total experimental process can be described by:

$$ep \rightarrow e' \gamma p' \quad (1.2)$$

This reaction has to take place in the *deep virtual limit*, defined by the following criteria:

 $Q^2 \gg M^2$, with Q being the *virtuality* (or the four-momentum transfer) of the virtual photon, and M the mass of the proton. When this condition is met, the photon is called *highly virtual*.

- $|t| = (p - p')^2 \ll Q^2$, with p and p' being the momenta of the initial and final proton respectively, and t representing the total momentum transferred to the proton.

In this limit, a global view of the process is given by the *handbag diagram* shown in figure 1.3.

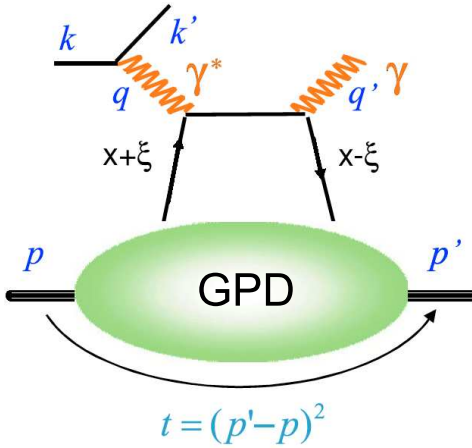


Figure 1.3: Handbag diagram of the DVCS process.

According to the handbag diagram, a single quark is kicked out of the proton with a strong acceleration by a virtual photon γ^* and carries out with it a fraction $x + \xi$ of the momentum of the nucleon. This quark then emits a real photon γ in order to lose energy and get back into the nucleon, however this time it brings back with it a different momentum fraction $x - \xi$. In this case,

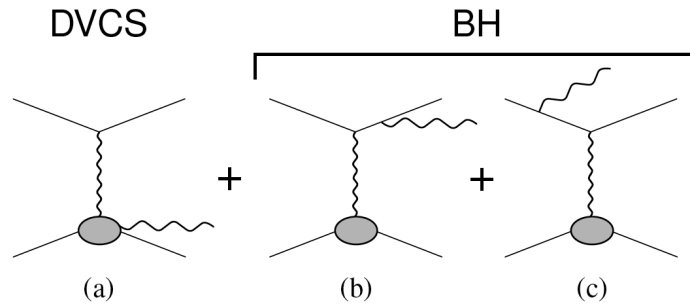


Figure 1.4: DVCS and BH processes are both characterized by $ep \rightarrow e'\gamma p'$.

x can be interpreted as the momentum fraction carried by the quark, and ξ as the longitudinal momentum fraction transferred to the proton.

The DVCS process isn't the only one to be described by the equation 1.2. A concurrent process called *Bethe-Heitler* (BH) can also happen and result in the emission of a real photon. In the BH process, the real photon is not emitted by the proton, but either by the incoming or outgoing electron. However, this process is completely calculable by the Quantum Electrodynamics equations.

Since the DVCS and BH processes lead to the same final quantum state, they create interferences as shown in figure 1.5. By exploiting these interferences, we can gain information about the GPDs. In order to do this, we use a polarized beam at 5.75 GeV to measure the cross-section difference for electrons of opposite helicities. The helicity can be understood as the projection of the spin of the electron on its momentum. It can be shown within the theoretical framework of the GPDs that this cross-section difference is proportional to the interference of the imaginary part of the DVCS amplitude, and the purpose of the E00-110 experiment is to measure this observable.

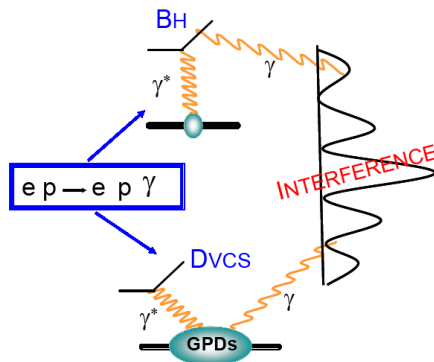


Figure 1.5: DVCS and BH processes interfere like in holography.

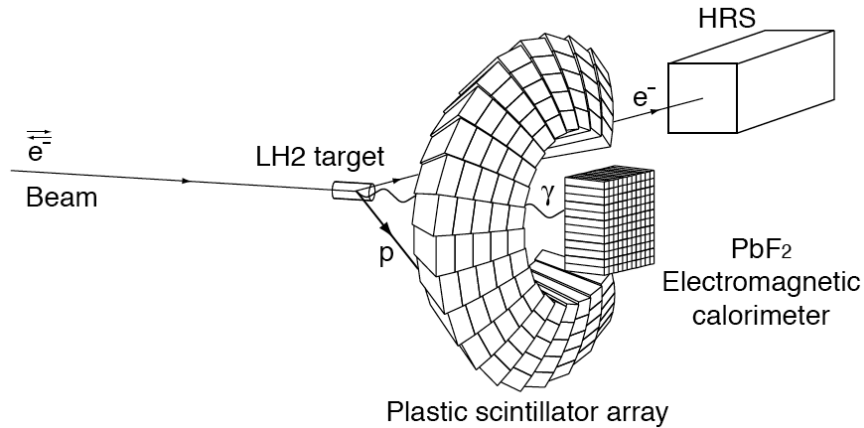


Figure 1.6: General setup of the DVCS experiment.

1.4 Experimental apparatus

1.4.1 General setup

For the DVCS experiment, the photon, the electron and the proton are going to be detected in coincidence (section 2.3.3 has more information about coincidences). As seen in the figure 1.6, the experiment uses a liquid hydrogen cryogenic target (see section 1.4.2), the Hall A High Resolution Spectrometer to detect the electron (see section 1.4.3), and a detector specifically built for the experiment composed of a calorimeter to detect the photon (see section 1.4.4) and of an array of plastic scintillators to detect the proton (see section 1.4.5).

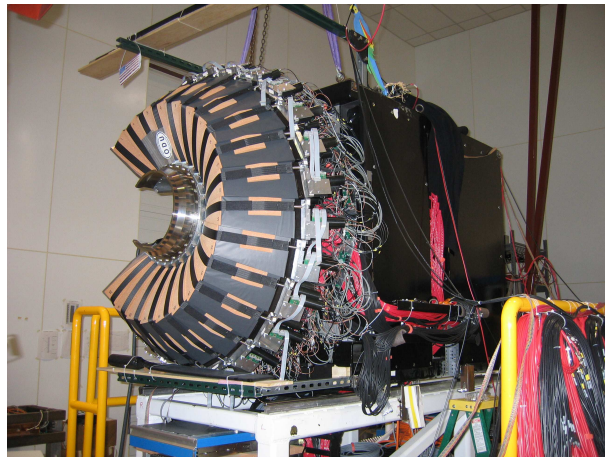


Figure 1.7: DVCS detector in the testing room.

1.4.2 Cryogenic target

The Hall A cryogenic target system actually consists of independent target loops: a liquid hydrogen (H_2) loop and a liquid deuterium (D_2) loop. The targets are arranged in a vertical stack which can be moved with a servoed target motion system. Besides the cryogenic targets, 3 dummy targets and 5 solid targets are available.

For the “E00-110” experiment, we are using the liquid H_2 target enclosed in a vacuum scattering chamber. This target is cooled down to 19 K by the helium supplied by the Central Helium Liquifier (see section 1.2.2). Its pressure is monitored through pressure transducers in several locations of the loop. The liquid D_2 target cooled down to 22 K will be used for experiment “E03-106: DVCS on the neutron”.



Figure 1.8: Scattering chamber in the storage building.

1.4.3 Hall A high resolution spectrometer

Presentation of the HRSs

The Hall A is equipped with two High Resolution Spectrometers (HRSs) called the Electron (HRSe) and the Hadron (HRSh) spectrometers. These very large detectors can be moved clockwise or counter-clockwise around the Hall A central pivot where the target itself is located. They have a minimum angle of 12.5° and a maximum angle of respectively 144.5° and 133.5° relatively to the beamline.

The spectrometers can measure and select the momentum of the scattered particles with a high precision: their resolution $\Delta p/p$ equals to 10^{-4} . However, they only cover a limited solid angle of 6 msr. The HRSs are primarily made of three quadripoles (Q1, Q2 and Q3) and of one dipole (D) arranged in a QQDQ configuration. Q1 provides dispersive (vertical) focusing, Q2 and Q3 transverse (horizontal) focusing. The magnetic dipole bends by 45° the trajectory of the particles entering the spectrometer and selects accurately their momentum.

The particles are then detected in the shielded “detector hut” localized at the top of the spectrometer: their trajectories and momenta are determined by two

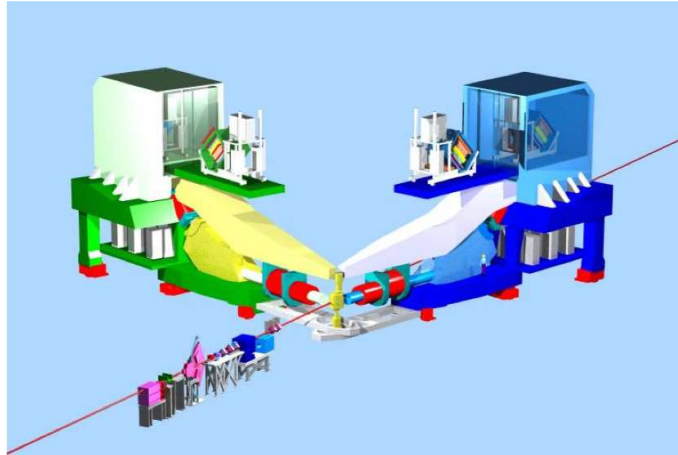


Figure 1.9: High Resolution Spectrometers in Hall A.

vertical drift chambers, and their time-of-flight is measured by two scintillator planes (named S1 and S2). Additionally, a gas Čerenkov detector and a lead glass preshower and shower counter are used for e^-/π^- separation.

HRs and the DVCS process

For the DVCS experiment, we cannot use both spectrometers to detect the outgoing particles. As seen on the figure 1.10, the reaction happens on two different planes: the leptonic plane which contains the trajectory of the scattered electron, and the hadronic plane the emitted photon and recoil proton. The cross-section difference that the experiment aims to measure varies in function of $\sin(\varphi)$, φ being the angle between these two planes. In other words, the observable is not ~~null~~ only if the outgoing proton is out of the electron scattering plane, and the High Resolution Spectrometers cannot detect such particles.

null -> zero

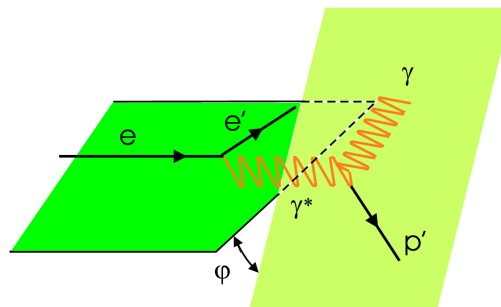


Figure 1.10: DVCS kinematics: leptonic (green) and hadronic (yellow) planes.

Therefore, we are using the Electron spectrometer to detect the electron and are replacing the Hadron spectrometer in its functions by a detector with a larger acceptance (see section 1.4.5). Actually, this HRS, pushed to its largest

angle, is only used as a tool to monitor the event rate.

1.4.4 Calorimeter

Purpose and characteristics of calorimeters

Calorimeters are particle detectors used to find the momentum \vec{q} of an incoming particle, which can be calculated by determining its energy and the position where it hits the detector. The main particularity of calorimeters is the fact they are made of a material thick enough to absorb nearly all of the particle energy in *showers* (see later for more information about these showers). They are nowadays used in all the large nuclear physics experiments. Two kinds of calorimeters can be distinguished: “true” and pseudo calorimeters. True calorimeters are making temperature measurements (hence the name calorimeter), while pseudo calorimeters detect other processes that are proportional to the energy.

The first true calorimeters date back from 1930. They can detect the energy of the incoming particle by measuring the temperature change of the absorber according to the following formula:

$$\Delta T = \frac{E_0}{c.M} \quad (1.3)$$

E_0 being the energy of the incident particle, c the calorific capacity of the calorimeter material and M its mass. However, this temperature variation can be low for limited incident fluxes, and thus hard to measure with accuracy.

Pseudo calorimeters usually detect light with an optical readout using photomultipliers or avalanche diodes. Light is produced through two processes: the Čerenkov process, which is described in the next section, and the *ionization* process which happens when a charged particle hits a particular family of materials called *scintillators*. Calorimeters can either use both effects or only the Čerenkov process.

Calorimeters are usually made of a matrix of separate elements having the same properties, as seen in figure 1.11. Their most important characteristics are energy resolution ($\frac{\sigma E}{E}$), their spatial resolution (σx), their time resolution and of course, their cost. We will review shortly the meaning of these characteristics in the case of *pseudo calorimeters with an optical readout*.

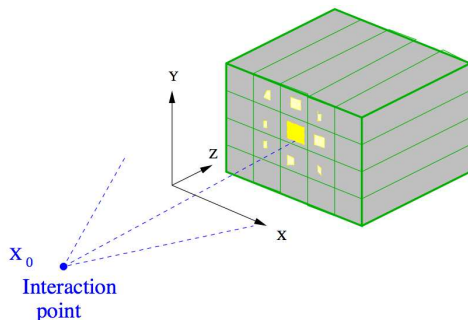


Figure 1.11: Structure of a generic calorimeter.

The energy resolution of a calorimeter depends greatly on the material used. For detectors using an optical readout, there is a wide range of materials available having each different characteristics, from crystal scintillators such as $PBWO_4$ to Čerenkov materials like glass. Typically the scintillators are characterized by a better energy resolution, but in fact the choice of the material is always a tradeoff between energy resolution, time resolution, price, and other factors (such as radiation hardness).

The spatial resolution is the accuracy of the detector when determining the location that was hit by the incident particle. It is directly linked to the size of the blocks used to build the matrix. One could think the best way to build a calorimeter would be with very small elements in order to increase the resolution. But this is not always the case, because:

- When a particle hits the calorimeter, it deposits energy not only in the block that was hit, but also in the surrounding blocks. The number of the elements involved is characterized by the *Moliere radius* $R_{Moliere}$: every block within this radius around the location of the impact will get a part of the energy. Therefore, we can achieve a higher resolution than just the width of the block by analyzing the amounts of energy deposited in the surrounding elements (see figure 1.12).
- Consequently, smaller blocks means that more elements will actually get a part of the incoming particle energy. The values of the energy deposited in each block needs to be read by the *data acquisition system* (DAQ), and as we will see in section 2.3 a too large amount of data to read can result in *DAQ dead times* during which the calorimeter cannot be used, and incoming particles missed.

The time resolution, or the rate at which incoming particles can be detected is linked to several factors:

- the scintillating time constant τ , during which the material emits light,
- the bouncing of the light in the block,
- the time resolution of the photodetector.

If several particles hit the same block during τ , the energy of these events cannot be resolved, and are thus lost. Usually, $\tau = 300ns$ for a scintillator such as BGO, and $\tau \approx 100$ for a Čerenkov crystal.

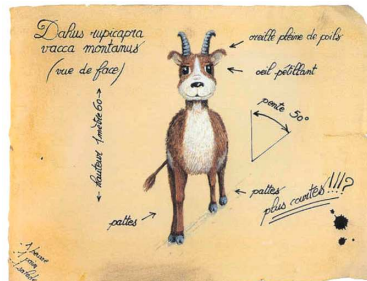


Figure 1.12: Several blocks within the Moliere radius are hit.

The DVCS calorimeter

As it has been previously said, the DVCS calorimeter has been built specially for the experiment. Centered along the direction of the virtual photon and placed at 110 cm from the target, it is made of 132 blocks arranged in 11 columns of 12 blocks. A block itself is a parallelepiped in PbF_2 crystal of $30\text{ mm} \times 30\text{ mm} \times 184\text{ mm}$. The block length corresponds to 20 radiation lengths³ in order to make sure that the DVCS photon loses all its energy when going through the calorimeter. Moreover, blocks are surrounded by white paper to diffuse light and black paper to avoid light leaks. Since $R_{Moliere} = 2.2\text{ cm}$, on average when a photon hits the center of a block 95% of its energy is absorbed by the central block, and the rest in the 8 surrounding blocks. Each crystal is linked to a photomultiplier (PMT) with optical grease.

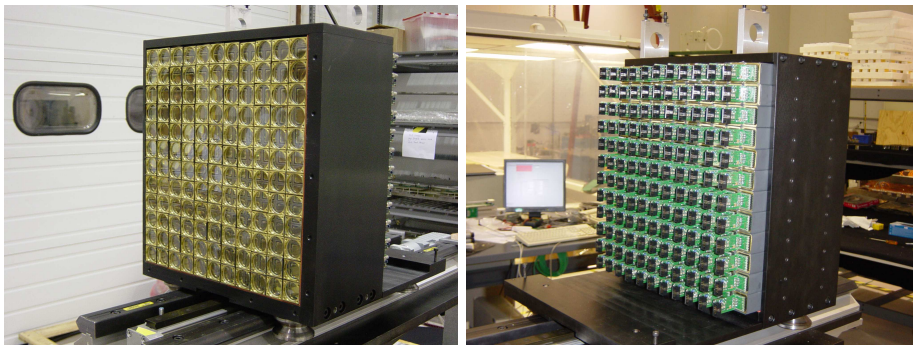


Figure 1.13: DVCS Calorimeter in the testing room: front and back view.

Photomultipliers are sensitive detectors of light having a maximum quantum efficiency for wavelengths ranging from 300 to 500 nm in our experiment. They are a type of vacuum tube in which photons produce electrons in a photocathode in consequence of the photoelectric effect and these electrons are subsequently amplified by multiplication on the surface of dynodes. The amplification factor can be as much as 10^8 .

When a real DVCS photon enters the crystal the *pair production* process occurs: the photon is converted into a pair of an electron and a positron.

$$\gamma \rightarrow e^+e^- \quad (1.4)$$

These particles then lose energy by *bremstrahlung* and emit photons. Bremsstrahlung (coming from the German for braking radiation) is the electromagnetic radiation produced by the deceleration of a charged particle when deflected by another charged particle, in our case the atomic nucleus of the lead glass.

$$e^\pm \rightarrow e^\pm\gamma \quad (1.5)$$

These bremsstrahlung photons also materialize themselves into a e^+e^- pair, that create photons by bremsstrahlung, and so on. This is the process creating the electromagnetic shower, as seen of figure 1.14. The total energy of the shower corresponds to the energy of the incident DVCS photon.

³The radiation length is defined as the distance over which a particle loses on an average 64.3% of its energy.



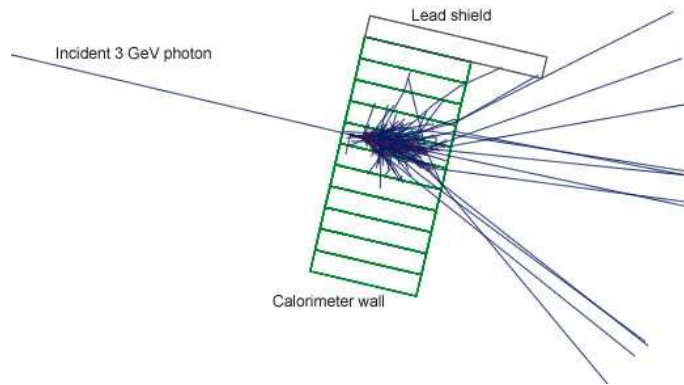


Figure 1.14: Shower resulting from a photon hit.

We use Čerenkov light to measure the shower energy. The Čerenkov effect happens when a charged particle exceeds the speed of light in a dielectric medium through which it travels⁴, and results in the creation of a photonic shockwave (see figure 1.15). In our case, the e^+e^- pairs produce a number of Čerenkov photons proportional to their number, and so to the total energy of the shower. These photons are detected by the PMTs at the end of the crystal, and converted into an electric signal. Section 2.3 will explain what happens to this signal after it has been generated.

Finally, the calorimeter is enclosed in a back box to prevent parasite light from reaching it.

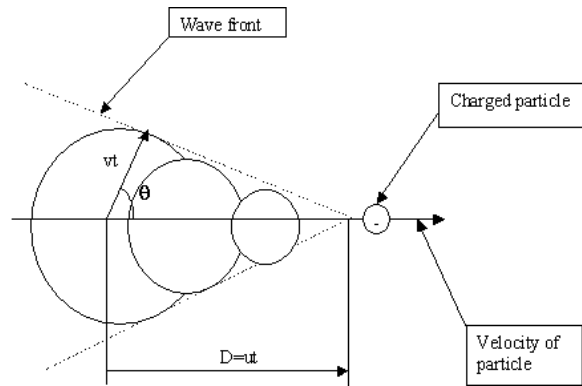


Figure 1.15: Čerenkov shockwave.

⁴While the relativity holds that c , the speed of light in the vacuum is an universal constant and cannot be exceeded, the speed of light *in a material* can be significantly slower.

1.4.5 Proton array

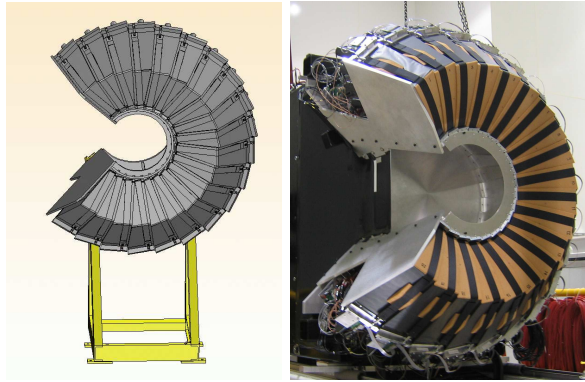



Figure 1.16: Proton array schematics (left) and actual view (right).

A detector made of blocks of plastic scintillator has been built to detect the proton. The blocks themselves are arranged on 5 rings of 20 blocks going from 45° to 315° in the azimuthal angle, and from 18° to 38° in the polar angle relatively to the detector axis. As the calorimeter, the proton array is centered along the virtual photon direction. The lack of blocks between is intended to let room on the path of the unscattered electron beam (see figure 1.17).

When a proton goes through a block, it ionizes the molecular states of the scintillator. The light coming from the decay of the excited states are then recorded by PMTs coupled to the end of each block, and characterizes the energy of the proton. 

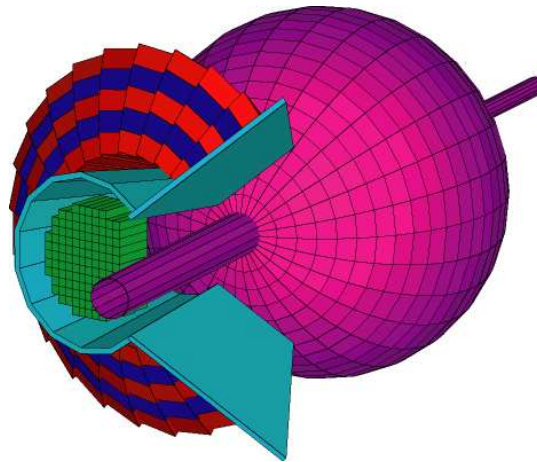


Figure 1.17: Scattering chamber and beamline (in purple) position relative to the calorimeter (green) and proton array (red and blue).

1.4.6 Tagger

The experiment “E03-106: DVCS on the neutron” uses a deuterium target, which means that incident electrons can be scattered off protons as well as off neutrons. As both the proton and the neutron induce ionization and therefore scintillation in the plastic scintillator array, the tagger has been devised in order to distinguish them.

The tagger detector is made of 2 layers of 20 thin (20 mm) paddles of scintillator connected to PMTs. As seen in figure 1.18 the tagger is located just in front of the proton array so that each paddle covers 5 proton array blocks. In this setup, an incoming particle must pass through one of the tagger elements before hitting the proton array. The neutron induces ionization when it kicks a charged particle such as a proton in the scintillating plastic. The thinner the scintillator is, the lower the probability of an interaction between the neutron and a charged particle is. The thickness of the paddles has been chosen with this property in mind. Therefore, whenever a photon is detected in the calorimeter, we check if the signal in the tagger is over a particular threshold: in this case, we know that the incident particle was a proton. On the contrary, if the signal is under the threshold we can infer that a neutron went through the tagger.

The tagger includes an iron shielding with a thickness of 10 mm in front of the paddles to discard the parasite low-power particles produced by other processes.

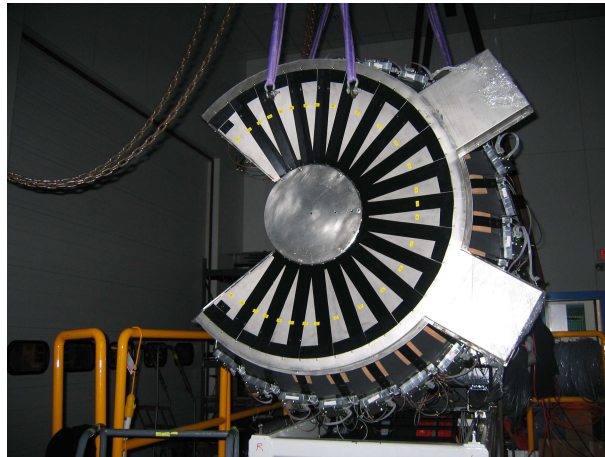


Figure 1.18: Tagger in position over the proton array.

Chapter 2

Several aspects of my work on DVCS

2.1 Timeline

My training period spanned over three months, from July 5th till September 29th. When I initially arrived at the Jefferson Lab, the detector was under final review in the testing room. My first month was mostly dedicated to getting used to the tools previously developed for the DVCS experiment, and to the initial calibration stages of the calorimeter (see section 2.2 for more information on this process). During the month of August, I moved on the more technical issue of data acquisition (see section 2.3 to learn about DAQ), a subject on which I would be working until the end of my internship. I chose here to develop more in detail these two aspects of my training period.

However, such a summary is only able to give a partial idea of the course of my work on the DVCS experiment. After the detector stack was moved to its final destination in the Hall A on August 16th, a large part of my work consisted in helping with the commissioning of the experiment which consisted in making sure that the detectors were functioning correctly and that the experiment was ready to begin. As only two weeks were available to test the three new detectors and any delay would reduce the time dedicated to data taking, this was perhaps the most critical moment for the DVCS experiment which had been in the works **for more than 3 years**. This was also the most challenging aspect of my training period: fixing the problems that arose daily imposed to have an accurate understanding of the interactions between the different subsystems of the detectors. It also involved an intense cooperation between all the members of the DVCS team. In this respect, the commissioning gave me the occasion to work on almost every aspect of the experiment.

2.2 Calorimeter calibration

2.2.1 The need for a calibration

The information we get from the detectors are actually electric pulses produced by the PMTs. These signals get converted into numeric values on an arbitrary

presque 5ans !

scale and recorded by the electronics and data acquisition systems. If we want this data to be meaningful, we have to know how to make the correspondance between numerical values and the physics events. This is the *absolute calibration* process, which is essential to every nuclear physics experiment. A physics process of a known energy is usually used to conduct absolute calibration. In fact, another calibration process is critical: the *cross-calibration*, which is the relative calibration of each calorimeter block in relation to the others. While all the calorimeter blocks have been designed to behave similarly, they are not rigorously identical. The crystals, photomultipliers, amplifiers and even the DAQ electronics exhibit small differences from one block to another that cannot be dismissed. Therefore, by default each block does not generate the same signal for the same stimulus. The goal of cross-calibration is to make the response of the calorimeter constant across the whole detector.

An important part of my work was centered around cross calibrating the DVCS calorimeter.

2.2.2 Cross-calibration using cosmic rays

At first, we used cosmic rays to cross-calibrate the detector. Cosmic rays are energetic particles originating outside of the Earth. Their composition includes electrons, protons, neutrons, and atomic nuclei from a large region of the periodic table. The kinetic energies of these particles span over fourteen orders of magnitude. The wide variety of particle energies is reflected in the wide variety of sources. Cosmic rays originate from energetic processes on the Sun all the way to the farthest reaches of the visible universe.

A lot of particles are reaching the earth at any time, but only the high-energy particles are actually able to go through the atmosphere and the roof of the laboratory. We can detect cosmic reaching the calorimeter by positioning around the detector plastic scintillator paddles read-out using PMTs, in the same manner as for the scintillator array described earlier (see section 2.3.3 for more information). When hitting the detector, they make showers in the blocks and deposit energy just as a DVCS photon would. We can therefore visualize the path of cosmic by reading the amount of energy they left in the different blocks: the elements hit are arranged in straight lines going from the top to the bottom of the calorimeter, as pictured in figure 2.1.

Cosmic rays can go through the calorimeter with any angle, but only a specific set of them is of interest in order to calibrate the detector: cosmic coming in vertically. In this configuration, all the blocks hit by the particles get the same amount of energy for the following reasons:

- the particle traveled the same length in each block,
- all the cosmic above a particular energy are depositing the same energy in the calorimeter (see figure 2.2).

Therefore, we took several sets of *cosmics runs* during which we let the detector record cosmic events. These were usually taken nightly, but in some cases could take as long as two days. The data of these runs was then analyzed using classes specifically developed for the DVCS experiment and written using the ROOT C++ libraries (see appendix B.4 for more information about the ROOT framework). The first part of the analysis consisted in characterizing

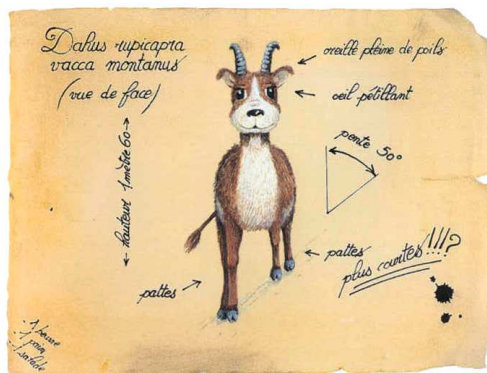


Figure 2.1: Event produced by a cosmic in the calorimeter, viewed from the back. The numbers represent the values of the energies that were deposited in each block.

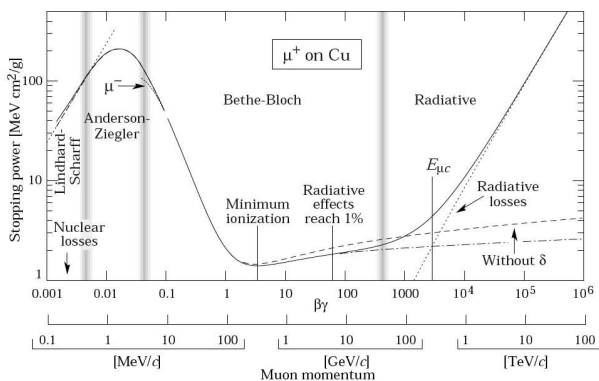


Figure 2.2: Stopping power of muons in copper. Cosmics in lead glass present the same profile, with a flat zone around the minimum ionization energy.

and selecting the events produced by the vertical rays. The criterion was simple: a cosmic was considered vertical if the elements in which it deposited maximal energies were arranged in a column. Such an event can be seen in figure 2.3. The second part consisted in adjusting the amplification factors of the blocks by changing the high voltages supplied the PMTs in order to get closer to equalizing all the energy values recorded in the column. The following formula to compute automatically the voltages was used:

$$\begin{cases} HV_i^{new} = HV_i^{old} * C_i \\ C_i = \frac{mean_i}{mean_{ref}} \end{cases} \quad (2.1)$$

with HV_i^{new} being the new high voltage of the block #i, HV_i^{old} the high voltage used during the run for block #i, $mean_i$ the mean of the integrated charges in block #i, and ref the number of the reference block (arbitrarily chosen as 39).

By iterating the process several times (taking runs, and analyzing them), we could cross-calibrate the whole calorimeter.

An histogram picturing the means of the integrated charges in all the different blocks is displayed in figure 2.4. This histogram can be fitted by a gaussian centered on the mean μ and having a standard deviation of σ . The parameter σ/μ characterizes the accuracy of the cross-calibration. For cosmics, we reached a value of 2.7% for σ/μ .

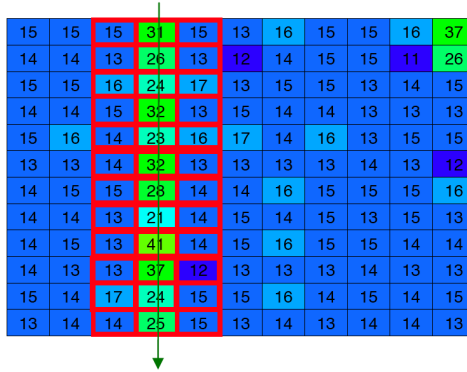


Figure 2.3: Event produced by a cosmic passing through the calorimeter vertically. The goal of cross-calibration is to have all the energy values in the column equalized.

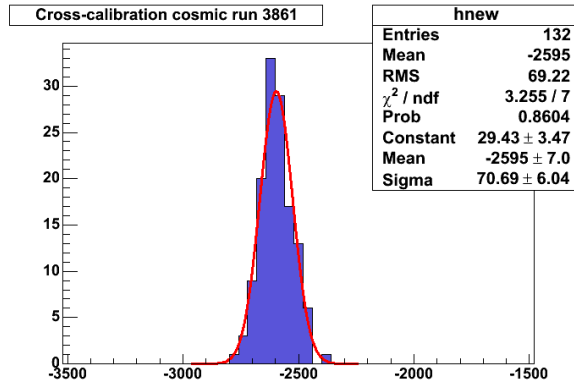


Figure 2.4: Histogram of the means of the integrated charges on each block for cosmic calibration and fitted gaussian ($\sigma/\mu = 2.7\%$).

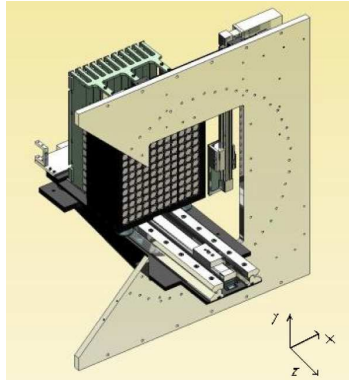


Figure 2.5: Schematics of the XY table.

2.2.3 Cross-calibration using LEDs

XY table description

Another way to cross-calibrate the calorimeter is by using a LED device mounted on an motorized *XY table* in front of the detector. As seen on figure 2.5, the XY table can be moved along the X axis, Y axis while the calorimeter itself can move along the Z axis. 4 different LEDs are placed of the XY table as seen on figure 2.6. The LEDs #1, #2 and #3 are pulsed LEDs which simulate the Čerenkov light. The 4th LED is continuous to simulate the ambient noise.

The light produced by the LEDs is conducted by a light guide in plexiglas to the collimator which is used to have parallel light rays. A pulser is used to light the Čerenkov LEDs in a predefined sequence:

LED 1, LED 2, LED 1+2, LED 3, LED 1+3, LED 2+3, LED 1+2+3

This allows us to check the linearity of the photomultiplier response to signals.

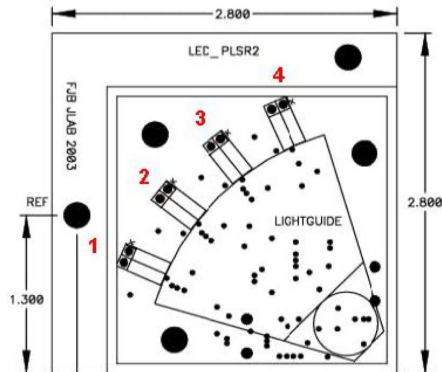


Figure 2.6: LEDs device on the XY table.

The XY table is controlled through the EPICS¹ slow-control². system. We control the table through *EPICS variables*. When one wants to move the table, one communicates with a dedicated Input-Output Controller (IOC) and sends it the new values of EPICS variables such as the target position in X through the network. In return, the IOC broadcasts on the network at regular intervals of times EPICS variables that allows us to monitor the behavior of the table, like the current position in X. Almost every apparatus in Hall A from the High Resolution Spectrometers to the cryotarget use EPICS for control.

Finding the center of the blocks

In order to ensure that the LED scan is relevant, ont has to check that the LED is at the same position in front of a block for every scanned block. Even if the mechanical detector stack was carefully built, there was no strict guarantee that the XY table and the calorimeter itself were perfectly aligned, or that no angle between their reference frames was introduced during the construction. That is why we conducted a *fine block scanning* in order to find the center of each element in the reference frame of the XY table.

ont -> onE

The “pseudo center” of a block was defined as the position corresponding to the maximum response of the PMTs when LED 1+2+3 were lit. This area might not be the geometrical center of the block because of the shape of the photocathode, but should be the same for each element of the calorimeter. The procedure to find the center would be the following: for each block “center” that needed to be determined, the XY table was programmed to scan a block by steps of 2 mm. For each position, the table stopped and the LEDs were lighted up. The table stayed for 5 seconds in each position in order to get a significant number of events.

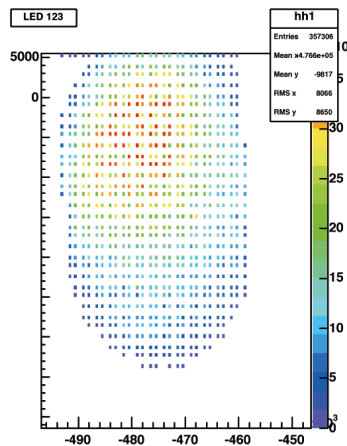


Figure 2.7: 3D maps of the block #131 produced by the fine-block scanning (top-down view).

¹Experimental Physics and Industrial Control System.

²This kind of control is called slow because it usually works at a low frequency (typically around 1Hz) compared to the DAQ (1GHz in our experiment)

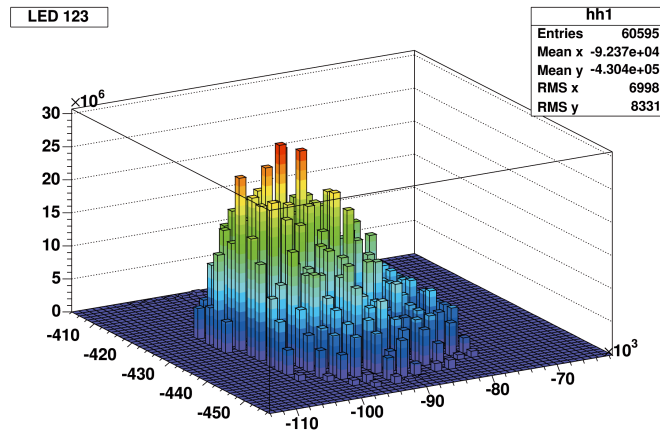


Figure 2.8: 3D maps of the block #131 produced by the fine-block scanning (isometric view).

After analysis, 3D-maps of the blocks were obtained as shown in figure 2.7 and 2.8. The pseudo center was fitted by a 2D gaussian. One interesting aspect of this method was that 3 blocks really needed to be scanned in order to obtain the whole calorimeter position matrix. The fine-scanning of the blocks corresponding to the corners of the calorimeter make it possible to know accurately the length between the position and the tilt of the whole calorimeter, and it is then possible to interpolate the pseudo-centers of the other blocks as the dimensions of the crystals are known precisely. The ultimate precision we achieved on locating the position of the pseudo-centers was ± 2 mm.

The goal of LED scans

Once the position of the pseudo-centers of the blocks has been determined, this information could be used to cross-calibrate the calorimeter with the XY table. The XY table only had to be positionned over the pseudo-centers, wait for 5 seconds with the LEDs lighted on and be moved to the next block. The high voltages supplied to the PMTs could then be adjusted with the same method that was used for cosmics in section 2.2.2. We reached here a value of σ/μ of 4.5%.

However, one can wonder what was the purpose of this additional calibration as we already got cross-calibration information from the cosmic rays. The point is that both approaches have their respective flaws as both do not create the same effects in the calorimeter as the DVCS photon: on one hand, while the cosmics create physical showers in the blocks through Čerenkov effect, they actually enter the crystals from *above* instead of from the front, and thus the photons are subject to many reflections before reaching the photocathode. On the other hand, while the LED is placed in front of the blocks, it *simulates* the Čerenkov effect by sending pulsed light, and the precision of its placement is critical. Which approach is the best is still open to interpretations (and simulations), as they give slightly different results for the position of the pseudo-

centers.

Nevertheless, the LED scan has a decisive advantage over cosmics: a full calorimeter scan doesn't take more than 25 minutes. Therefore, it can be used to monitor the drift of the response of the blocks while the experiment is running. This drift is mainly caused by two factors: the progressive opacification of the crystals when they are struck by radiation (this effect can be partially reversed by using ultra-violet lights on the calorimeter elements) and by the wear up of the PMTs. On several blocks, the gain variation can be as much as 30% in 20 days of run as pictured by figure 2.9. Knowing the amount of drift allows us to compensate this effect by hardware (adjusting again the high voltages) or software.

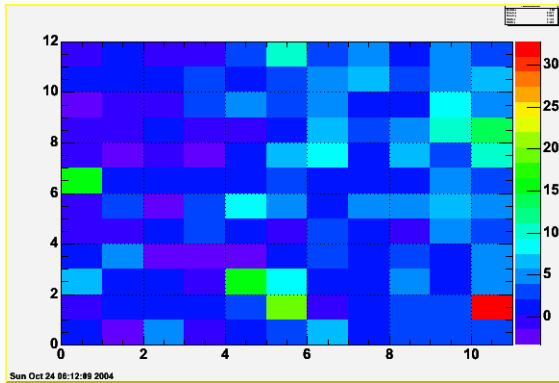


Figure 2.9: Gain variation over 18 days of the different calorimeter blocks. 4 blocks are above 15%, and one above 30%.

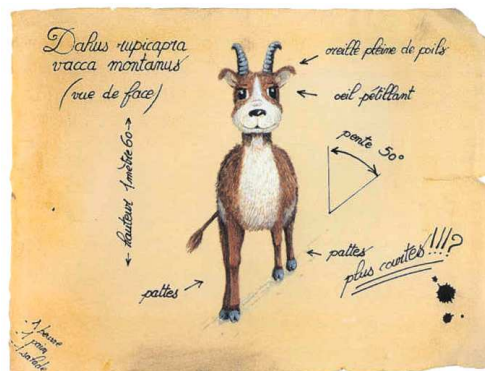


Figure 2.10: Gain variation over 18 days of block #39.

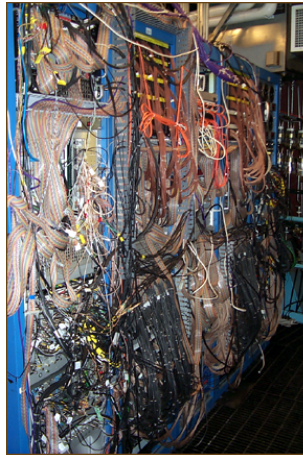


Figure 2.11: Hall B DAQ system. Removing a single cable is likely to cause the failure of the whole system.

2.3 Data acquisition

2.3.1 Challenges of data acquisition

Data acquisition is one of the hidden aspects of any modern nuclear physics experiment. The goal to any experiment is to gather data about nuclear interaction using specific detectors. When particles pass through these detectors, they generate signals which contain information about them, such as their type, energy or trajectory. The main goal of the DAQ system is to format and store this information in a way that can be retrieved for a later analysis. The tasks that the DAQ system has to execute include:

- triggering, which means choosing the events we want to record,
- digitizing the signals (called “events”) coming from the detector,
- formatting the events,
- putting fragments of events from each detector together,
- transporting the events to storage,
- storing the data,
- providing a way to monitor the whole process.

Speed is an important factor in DAQ systems. When an event is detected and sent to DAQ, the amount of time which is spent processing it is called *dead time*. As its name implies the detector is virtually dead during this timeframe: any new event will be ignored, which means that the corresponding physical processes will never get recorded. Since there can be several thousands of events per second, having dead times as low as possible is critical. There are not many ways to reduce dead times:

- using fast digitizing electronics, such as the ARS (see more about it in section 2.3.2),
- reducing as much as possible the operations blocking the DAQ.

In order to perform all these operations, DAQ systems are usually involving a huge number of electronic devices arranged in a complex configuration. Moreover, the configuration of the system can change greatly from an experiment to another. Because of this, DAQ systems are often seen as a real *mess* for people that didn't work closely on them, and are usually the first elements to be blamed if the experimental results differ from what was planned.

Nevertheless, DAQ is essential to nuclear physics experiments and I found it to be a very interesting aspect of the experiment.

2.3.2 Data acquisition electronics

Analog ring samplers

The Analog Ring Samplers (ARSs) are the main digitizing devices of the DVCS experiment, as they are used to record signals coming from the calorimeter, proton array and tagger. ARS were initially developed for the ANTARES³ experiment, but DVCS is the first. The ARS is basically an *analog memory* with a maximal sampling rate of 1 GHz. The signal coming from the PMTs is sampled every nanosecond on 128 condensers successively, giving an effective time window of 128 ns. The amplitude at each step of 1 ns can be digitized by an Analog to Digital Converter (ADC) on 12 bits (4096 values). The signal can then be reconstructed from the samples, like on a numeric oscilloscope.

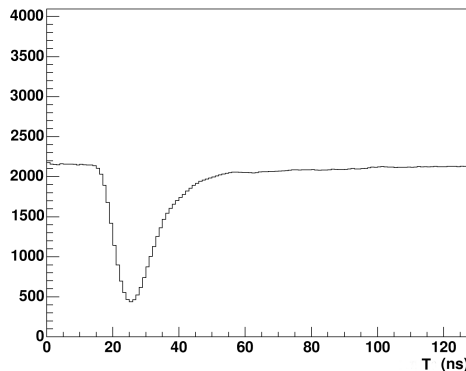


Figure 2.12: Typical pulse from a photomultiplier recorded by the ARS.

One of the most interesting aspects of the ARS is the fact that the sampling occurs continuously in a ring pattern, which means an old sample is overwritten by a new one on every nanosecond. The sampling stops when the ARS gets a signal on its STOP entry. Depending on how the device is set up, several things can happen:

³The ANTARES project aims to study very high-energy cosmic neutrinos using an underwater telescope in the Mediterranean Sea. The telescope will begin operation in 2006.

- the ARS can stop the sampling as soon as the STOP signal is received. In this case, the analog memory will have recorded the 128 ns anterior the STOP, or 128 ns “in the past”.
- The ARS can also be set up to continue the sampling for a predefined amount of time after the STOP, such as 40 ns. In this situation, the analog memory would contain 88 ns of “past”, and 40 ns of “future”.

The memory contents can then be digitized when the ARS gets a signal on its VALID entry, or discarded by a signal on its CLEAR entry. These abilities give the ARS a flexibility that is uncommon for regular digitizing electronics. We’ll see in section 2.3.3 what are the uses of these features.

Another advantage the ARS has over the regular ADC + TDC (Time to Digital Converter) combination that is usually used in nuclear physics events is its ability to resolve pile-up problems at high counting rates. Even if two signals are generated by a PMT in the 128 ns window, one can be distinguished from the other as seen of figure 2.13

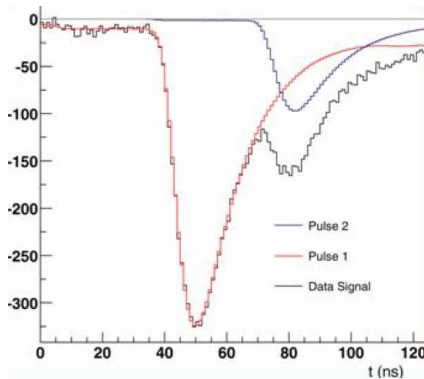


Figure 2.13: Example of a pile-up event that the ARS is able to resolve.

VME crates

All the electronics that are used for the DAQ system are modules and boards connected in several crates. These modules are linked together with cables and the crates own system buses. The dominant bus format that is used for the DVCS experiment is VME (VersaModule Eurocard). VME is a 64-bit bus developed by Motorola, Signetics, Mostek and Thomson CSF, going up to 80 MB/s⁴ It is mainly used for military and research applications.

Every data transfer on the bus is controlled by a system controller plugged in slot #1, which was for us a PowerPC CPU. The system controllers arbitrate the data transfers between the different cards on the VME bus, but can also directly address the registers of any device plugged in. We use the PowerPC CPUs as Read-Out Controllers (ROC), which means they have to extract the data from the ARS at the right time, format the events and send them over the

⁴VME64X provides up to 320 MB/s, but is not widely used yet.

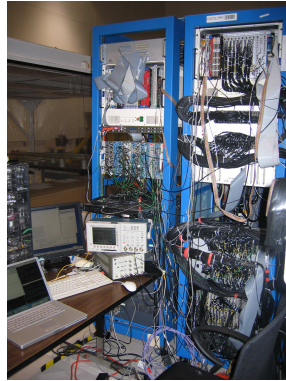


Figure 2.14: DVCS VME crates for DAQ in the testing room.

network. As we've seen previously the response time of the DAQ system is critical, therefore we cannot use a general purpose UNIX-like system but a *real-time* operating system (RTOS). A system is called real-time when it guarantees that the operation time of a specific task will be shorter than the maximum delay allowed in view of circumstances outside the operation. While there are many open-source or free RTOS (like RTLinux, RTAI or QNX), the commercial VxWorks from WindRiver is used on the DVCS PowerPCs. VxWorks is a popular RTOS for many devices and embedded solutions.

The main particularity of VxWorks is that it does not run development systems software such as compiler, linker and editor on the target machine. The development environment is based on cross-development or remote-development method. The compilers or debuggers are run on a remote UNIX machine, and the compiled application code is then uploaded dynamically in the physical RAM of the CPU boards through the network. While code for VxWorks can be developed in C or C++, real-time coding often require specific programming techniques.

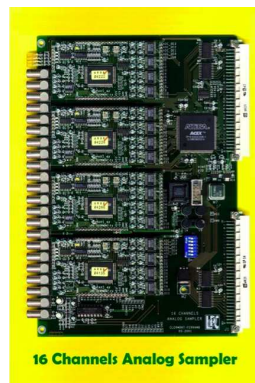


Figure 2.15: Side view of a VME ARS board. There are 4 ARS units with 4 channels each, giving a total of 16 channels per board.

2.3.3 Triggering procedure

When running an experiment, thousands of events can reach the detector in a second. Of course, in this huge number of events only a limited set interests us - in our case, the we only want to record the particles produced by a DVCS or BH reaction. Recording all the events is not practical: no electronic device would be fast enough to process them all with a good accuracy, and the amount of data generated would be tremendous. That is why we have to find a way to choose the events we want to record, a procedure which is called *triggering*.

Triggering basics: the coincidence

To get a better understanding on how triggering is working, let's study one of the most simple trigger configurations: the one that was used to calibrate the calorimeter with cosmics in section 2.2.2. As seen in figure 2.16, two scintillators paddles coupled to PMTs were placed above and under the calorimeter. A discriminator was connected to the PMTs in order to have a clean squared signal whenever a pulse from the PMT was detected to be over a specified threshold.

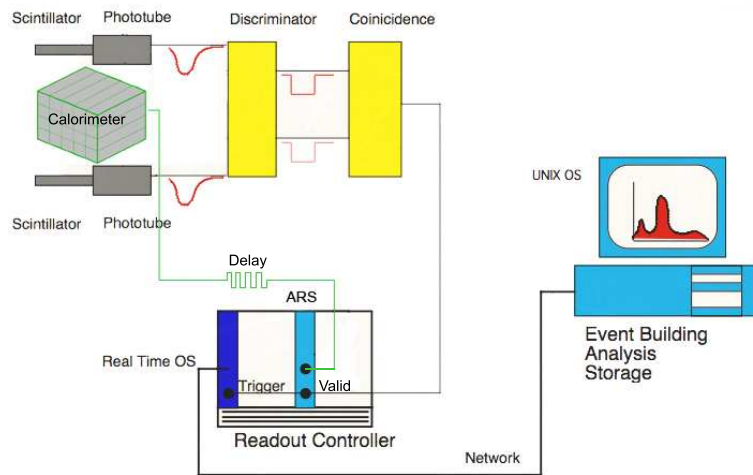


Figure 2.16: DAQ setup for cosmics.

When a cosmic ray hits the calorimeter in this configuration, it also passes through both scintillators which generate pulses. As we are only interested in cosmic events for these runs, data from the calorimeter must only be recorded when a pulse is detected at the same time on both paddles, which is called a *coincidence*. The coincidence detector will generate a signal only if it records a pulse coming from both scintillators in a predetermined time window. The signal coming out of the coincidence detector is our *trigger signal*. Connected to the VALID entry of the ARSs, it instructs the analogic memories to record the event.

The correct timing of the trigger system is vital. Obviously, if cables of different lengths are used to connect the paddles, the coincidences will not be

detected as the speed of the electric signal is not infinite. However, the propagation time of the signal in the logic gates of the discriminator and coincidence detector has to be taken into account or else, when the VALID command arrives to the ARS the signal coming from the calorimeter will already be lost ! Therefore, the calorimeter signal has to be *delayed*, and this delay needs to be of the same exact time that is spent detecting the coincidence and generating the trigger signal. The easiest way to do this is to add a length of cable measured by the time of propagation of a pulse, with the following formula :

$$t = \frac{2.l}{2/3.c} \quad \text{with } c = 3.10^5 \text{ m.s}^{-1} \quad (2.2)$$

For cosmics, the coincidence module is simple and thus relatively fast, however as we will see in the next section, significant delays need to be introduced when complex triggering modules are involved. Meters and meters of cables can be used this way, especially as we use one cable per channel !

Triggering in the DVCS experiment

The DAQ configuration that was used for actual data taking is more refined than the one used for cosmics, both at the scale of detectors and of the whole experiment. I will describe here its main characteristics and features.

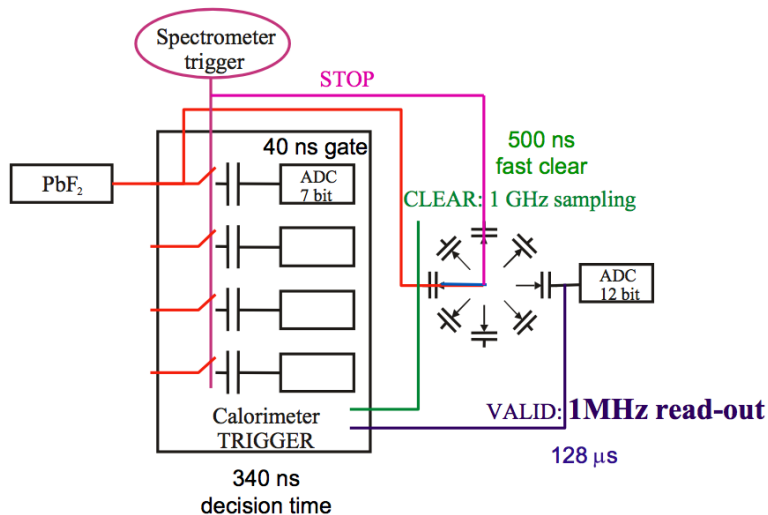


Figure 2.17: Schematics of the DVCS trigger.

At the scale of the calorimeter When a particle hits the calorimeter, we cannot read all the block channels at once because it would introduce too much dead time. In order to select which channels have to be read, a separate trigger module designed for the DVCS experiment is used. This trigger is directly connected to the calorimeter PMTs just like the ARSs, as seen in figure 2.17. When a particle is detected in the spectrometer, a STOP signal is issued to the

ARs which has the effect of freezing the data sampling of the PMTs output. The trigger module uses 7-bit flash ADCs to quickly digitize the signal coming from all the channels, and compute the integrated charges of the pulses in a 40 ns window. The trigger then proceeds to compute the sums of the charges integrated in the different “towers” of the calorimeter. These towers are actually groups of 4 blocks arranged in a square. All these operations are very quick: the decision time does not take any longer than 340 ns. If the value of a tower exceeds a predefined threshold, a VALID signal is sent to the corresponding ARs and the digitization of the signals on 12 bits occurs. 128 *mus* are spent during this operation. If no tower is over the threshold and thus there is no channel to read, a CLEAR command is issued to the ARs in order to resume the sampling. Since the CLEAR operation takes around 500 ns, less than 1 *mus* is lost by the DAQ system in this case.

At the scale of the experiment As it has been said previously, the DVCS process is characterized by the scattering of an electron, the kickback of a proton and the emission of a real photon. A set of independent trigger systems on each of the particle detectors wouldn't be able to select accurately the DVCS events from the others processes: the triggering has to be done at the scale of the whole experiment. A device called *trigger supervisor* which centralizes the different trigger signals is used in this purpose. The trigger supervisor orders the simultaneous recording of *all* the detectors when an event is detected in the HRS (a particle has gone through the scintillators S1 and S2) and in the calorimeter (there are towers that need to be read).

The proton array is working in *slave* mode, as it doesn't play an active role in triggering. In fact, as in DVCS kinematics the proton and the photon directions are opposite on both sides of the virtual photon path, the blocks that need to be read in the proton array during a DVCS event can just be determined by knowing the location the photon hit the calorimeter. A correspondance table between the calorimeter blocks and the proton array blocks has been created from the simulation results: on average, 23 proton array blocks are to be read during a DVCS event.

Conclusion

When it comes, the summer I spent working of the DVCS experiment has been an incredible experience. During these three months, I've had the chance to work on almost every aspect of a modern nuclear physics experiment, from simulation and calibration to actual cabling and repairing.

From the initial set-ups of the detector to the “final showdown” when the first beam was delivered to Hall A, the DVCS experiment has been a like a marathon which never stopped to take speed. And while there have been hard times and setbacks especially during the commissioning period, taking part in the first days of data taking and seeing the first concrete results was worth all the time and efforts that went into the experiment.

After the end of the experimental runs, another important will take place: the analysis of the data collected. I will not be involved in this part of the experiment, but I look forward to seeing in 2005 the final results and conclusions of the DVCS experiment.

Appendix A

ROOT framework

Appendix B

Examples of ROOT offline analysis macros

- B.1 Calibration with cosmics
- B.2 LED shape analysis
- B.3 Example of a VxWorks program
- B.4 Miscellaneous pictures